

# Molecular and cluster structures in $^{18}\text{O}$

W. von Oertzen<sup>1,a</sup>, T. Dorsch<sup>1,2</sup>, H.G. Bohlen<sup>1</sup>, R. Krücken<sup>2</sup>, T. Faestermann<sup>2</sup>, R. Hertzenberger<sup>3</sup>, Tz. Kokalova<sup>1,b</sup>, M. Mahgoub<sup>2</sup>, M. Milin<sup>4</sup>, C. Wheldon<sup>1,b</sup>, and H.-F. Wirth<sup>2,3</sup>

<sup>1</sup> Helmholtz-Zentrum Berlin, Glienicke Str. 100, D-14109 Berlin, Germany

<sup>2</sup> Physik Department E12, Technische Universität München, James-Frank-Str., D-85748 Garching, Germany

<sup>3</sup> Sektion Physik der Universität München, Am Coulombwall 1, D-85748 Garching, Germany

<sup>4</sup> Department of Physics, Faculty of Science, University of Zagreb, Bijenicka 32, HR-10000 Zagreb, Croatia

Received: 3 September 2009 / Revised: 15 October 2009

Published online: 4 December 2009 – © Società Italiana di Fisica / Springer-Verlag 2009

Communicated by N. Alamanos

**Abstract.** We have studied the multi-nucleon transfer reaction  $^{12}\text{C}(^7\text{Li},p)$  at  $E_{lab} = 44$  MeV, populating states in the oxygen isotope  $^{18}\text{O}$ . The experiments were performed at the Tandem accelerator of the Maier-Leibniz Laboratory in Munich using the high-resolution Q3D magnetic spectrograph. States were populated up to an excitation energy of 21.2 MeV with an overall energy resolution of 45 keV, and 30 new states of  $^{18}\text{O}$  have been identified. The structure of the rotational bands observed is discussed in terms of cluster bands with the underlying cluster structures:  $^{14}\text{C} \otimes \alpha$  and  $^{12}\text{C} \otimes 2n \otimes \alpha$ . Because of the broken intrinsic reflection symmetry in these structures the corresponding rotational bands appear as parity doublets.

## 1 Introduction

In light nuclei clustering and deformations are observed as general phenomena at excitation energies close to the  $\alpha$ -decay thresholds [1–4]. With the additional neutrons specific molecular structures appear, with binding effects based on covalent molecular neutron orbitals. This observation has been summarized in the “Ikeda” diagram for  $N = Z$  nuclei [1] in 1968, and for nuclei with extra neutrons in an extended diagram by von Oertzen [5]. In these diagrams  $\alpha$ -clusters and  $^{16}\text{O}$  clusters are the main ingredients. Actually, the  $^{14}\text{C}$ -nucleus has also equivalent properties as a cluster as  $^{16}\text{O}$ . These are: i) closed  $p$ -shells (even better closure than in  $^{16}\text{O}$ ), ii) the first excited states are at 6 MeV excitation energy, iii) the binding energies of nucleons are very high:  $E_B(p) = 20.83$  MeV,  $E_B(n) = 8.17$  MeV, iv) the binding energy for  $\alpha$ -particles is also high ( $E_B(\alpha) = 12.012$  MeV). Therefore pronounced clustering and molecular configurations with  $\alpha$ -clusters and neutrons are also observed in the oxygen isotopes with  $A \geq 18$ .

At present the  $\alpha$ -cluster structure for a number of low-energy states of  $^{18}\text{O}$  is reasonably well established. For  $^{18}\text{O}$  the literature [6] shows a large variety of reaction studies, as well as calculations, which established the level scheme and the main shell model structures. A number

of experimental studies were devoted to the direct investigation of the  $\alpha$ -cluster properties of the  $^{18}\text{O}$  nucleus close to the  $\alpha$ -decay threshold. Morgan *et al.* [7] populated  $\alpha$ -cluster states in  $^{18}\text{O}$  up to 12.5 MeV excitation energy with the  $^{14}\text{C}(^7\text{Li},t)$  reaction (at the beam energy of 20.4 MeV) and Fortune *et al.* [8] studied  $^{18}\text{O}$  using the  $^{12}\text{C}(^7\text{Li},p)$  reaction at 16 MeV. Cunsolo *et al.* [9,10] have measured  $^{18}\text{O}$  states up to 17.0 MeV excitation energy via the  $^{14}\text{C}(^6\text{Li},d)$  reaction at the  $^6\text{Li}$  beam energy of 34 MeV and performed a detailed analysis of the deuteron angular distributions. A study of  $\gamma$ -decays in the  $^{14}\text{C}(^7\text{Li},t,\gamma)$  reaction [11] has given strong evidence for enhanced  $E1$  and  $E2$  transitions. These are explained due to pronounced clustering as discussed in the present work, where the existence of parity inversion doublets is invoked. Angular-correlation studies of the decay of  $^{18}\text{O}$  states populated in the  $^{14}\text{C}(^6\text{Li},d)^{18}\text{O} \rightarrow ^{14}\text{C} + \alpha$  reaction have been used in the work of Artemov *et al.* [12,13] to extend the systematics of  $^{14}\text{C} \otimes \alpha$  cluster states in  $^{18}\text{O}$ . Finally, many of the spin values of resonances with a potential cluster structure above the  $\alpha$  threshold have been assigned via elastic scattering  $^{14}\text{C}(\alpha,\alpha)$  and the  $^{14}\text{C}(\alpha,n)$  reaction in the work of Morgan *et al.* [14]. The  $\alpha$ -decay of the states above the 6.226 MeV threshold has been observed by Curtis *et al.* [15] using the  $^{14}\text{C}(^{18}\text{O}; ^{14}\text{C}, \alpha)^{14}\text{C}$  reaction at an incident energy of 102 MeV. Several excited states were observed between 7.86 MeV and 16.42 MeV, and the energy-spin systematics of the states was extended. The molecular band in  $^{18}\text{O}$  with a  $(^{12}\text{C} \otimes 2n \otimes \alpha)$  intrinsic structure, proposed by Curtis *et al.* [15], has also been

<sup>a</sup> e-mail: oertzen@helmholtz-berlin.de

<sup>b</sup> Present address: School of Physics and Astronomy, University of Birmingham, Edgbaston, B15 2TT, Birmingham, UK.

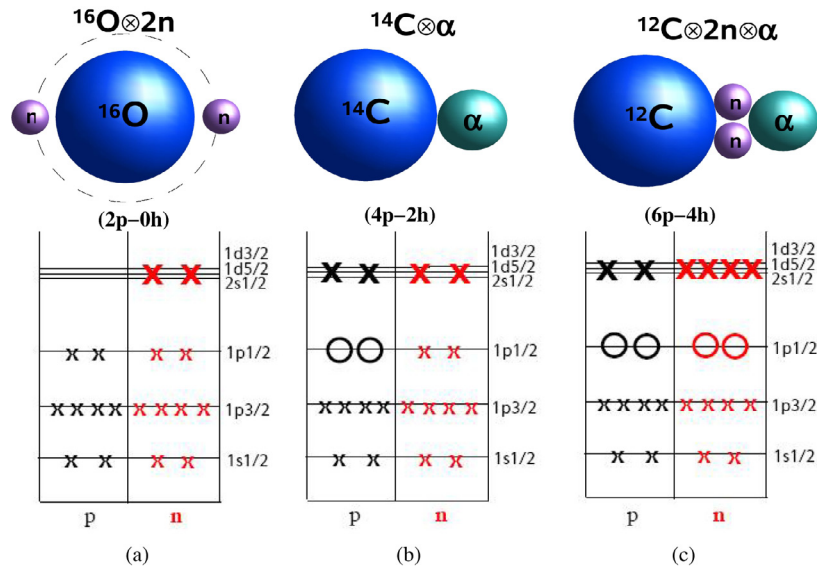


**Fig. 1.** (Color online) Cluster model structures (shown in the upper part) and corresponding shell model structures (lower part) of  $^{18}\text{O}$ . On the left the  $(^{16}\text{O} \otimes 2n)$  structure can be described by the shell model. The structure shown in the middle corresponds to an additional (2p-2h) excitation; it is also well described in the cluster model. The structure on the right requires a (6p-4h) excitation in the shell model, and a “molecular” configuration with two valence neutrons in the cluster model.

discussed earlier by Fortune *et al.* [16] in the framework of (6p-4h) shell model states. The missing  $0^+$  band head was predicted by Fortune *et al.* at 7.11 MeV, however, we have localized it at a different place (see sect. 2). Negative-parity  $\alpha$ -cluster states in  $^{18}\text{O}$  have been investigated by M. Gai *et al.* [17] and V. Goldberg *et al.* [18] giving indications for intrinsic reflection asymmetric shapes.

There are several theoretical publications addressing the formation of  $(^{14}\text{C} \otimes \alpha)$  cluster states in  $^{18}\text{O}$ , and the associated molecular bands, for example, by Lawson *et al.* [19], Lévai *et al.* [20], Reidemeister *et al.* [21] and Descouvemont and Baye [22]. More recently the AMD (antisymmetrised molecular dynamics) calculations of rotational bands by Furutachi *et al.* [23] form a useful quantitative basis for the comparison with the present measurements. The role of the valence neutrons being shared by all four  $\alpha$  giving rise to intrinsically symmetric states is discussed by Itagaki and Kimura [24], giving low-lying  $0^+$  states.

In the shell model frame work deformations and rotational bands appear as multi-particle–multi-hole excitations ( $xp-yh$ ). These are already well known in  $^{16}\text{O}$ , a (4p-4h) rotational band is well established starting at 6.05 MeV with the  $K = 0_2^+$  band head. The corresponding structures in  $^{18}\text{O}$  have (4p-2h) and (6p-4h) configurations [16]. In this work the emphasis was put on states with positive parity. The negative-parity states are related to odd numbers of particles and holes, in the shell model, *e.g.*, (1p-1h) or (3p-3h) for  $^{16}\text{O}$ . Similarly, the particle-hole structures of the negative-parity bands in  $^{18}\text{O}$  are, *e.g.*, (3p-1h) or (5p-3h). In the cluster model the negative-parity bands appear in these cases as a natural consequence of the intrinsic reflection asymmetry of the cluster configurations. The appearance of the parity inversion

band with negative parity was for the first time suggested for  $^{20}\text{Ne}$ , where for the  $^{16}\text{O} \otimes \alpha$  configuration in the ground state two bands are obtained: the  $K = 0_1^+$  ground-state band and the  $K = 0_1^-$  band [1]. They correspond to (4p-0h, 5p-1h) configurations in the shell model, respectively. In  $^{18}\text{O}$  the corresponding structures are (4p-2h, 5p-3h), these form excited bands.

With the parity projection of the intrinsic asymmetric cluster structures shown in fig. 1 for  $^{18}\text{O}$ , we obtain inversion doublets, *e.g.* for  $^{14}\text{C} \otimes \alpha$  two bands with quantum numbers  $K = 0_2^+$  and  $K = 0_2^-$ . Similarly we expect an inversion doublet for the cluster states with the  $^{12}\text{C} \otimes 2n \otimes \alpha$  configuration (in the shell model these will be (6p-4h) configurations). Here molecular orbitals for the valence neutrons appear. These covalent neutron configurations are also predicted in the AMD calculations, and were also found in the Ne-isotopes with masses  $A = 21, 22$  based on the  $^{16}\text{O} \otimes \alpha$  cluster structure, as discussed in ref. [5]. In earlier work on negative-parity configurations with cluster structure in  $^{18}\text{O}$  the emphasis was put on the  $^{14}\text{C} \otimes \alpha$  structure with intrinsic dipole and octupole moments and expectations of  $E1$ - $\gamma$ -transitions [17]. The intrinsic reflection asymmetry gives rise to rotational bands as parity doublets, with  $E1$ - $\gamma$ -transitions between the two bands. However, until now these structure effects have not yet been fully established.

In the present work [25] the multi-nucleon transfer reaction ( $^7\text{Li}, p$ ) on  $^{12}\text{C}$  is used, which can populate both, shell model states in  $^{18}\text{O}$  as well as those with cluster structure. We have studied the reaction with the aim to establish the higher-lying cluster states and find the corresponding inversion doublets and the high-spin members of the rotational bands. Due to the angular-momentum mismatch between the incoming and outgoing channels

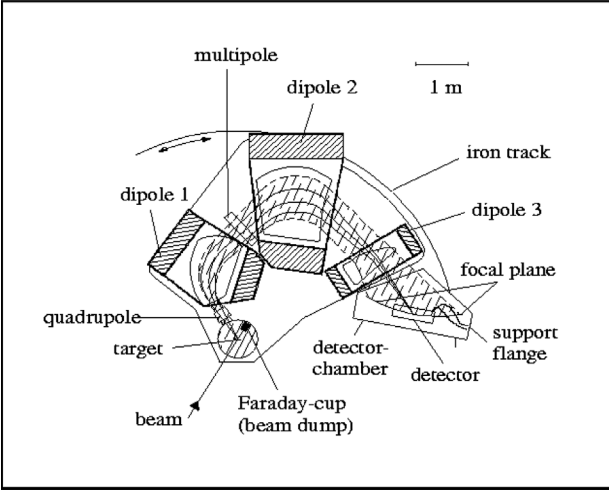


**Fig. 2.** The Q3D magnetic spectrograph used for the study of the reaction  ${}^7\text{Li} + {}^{12}\text{C} \rightarrow \text{p} + {}^{18}\text{O}$ , at  $E_{lab} = 44.0$  MeV.

(particles  ${}^7\text{Li}$  and  $\text{p}$  have very different mass, and the latter can carry only small amounts of angular momentum) the reaction is expected to populate strongly higher-spin states of the rotational bands. This is also true for a compound nuclear reaction mechanism. In addition, in direct reactions a strong population of states with cluster structures and high spin should be observed. Independently of the reaction mechanism for the population of states, we expect within the same band a dependence of the cross-section on  $(2J + 1)$ , the spin multiplicity. This feature, together with the energy systematics for rotational bands (dependence on  $J(J + 1)$ ) and the predictions of the AMD calculations are used to establish the rotational bands in  ${}^{18}\text{O}$ , with new, although preliminary, spin assignments.

## 2 The experiments

### 2.1 Experimental conditions, energy spectra

The experiments have been performed at the Tandem-van-de-Graaff accelerator of the Maier-Leibniz Laboratory of the Technische Universität München and the Ludwig-Maximilians Universität München. The incident energy of  ${}^7\text{Li}$  was 44 MeV, which allowed, together with the high positive  $Q$ -value of 8.401 MeV, the population of states up to high excitation energies. The  ${}^7\text{Li}({}^{3+})$ -beam intensity was typically about 200 nA. The  $({}^7\text{Li}, \text{p})$  reaction has been measured at the Q3D magnetic spectrograph [26] (see fig. 2) and the outgoing protons were identified by the focal-plane detector using the energy loss in a gas-filled chamber and the light output of a scintillator behind it. The position in the focal plane was established using the cathode strips read-out and ASIC<sup>1</sup> interpolation technique. Further details of the detector in the focal plane [27] and the experimental set-up are given in [25]. The  ${}^{12}\text{C}$  targets had a thickness of  $70 \mu\text{g}/\text{cm}^2$ , with an enrichment

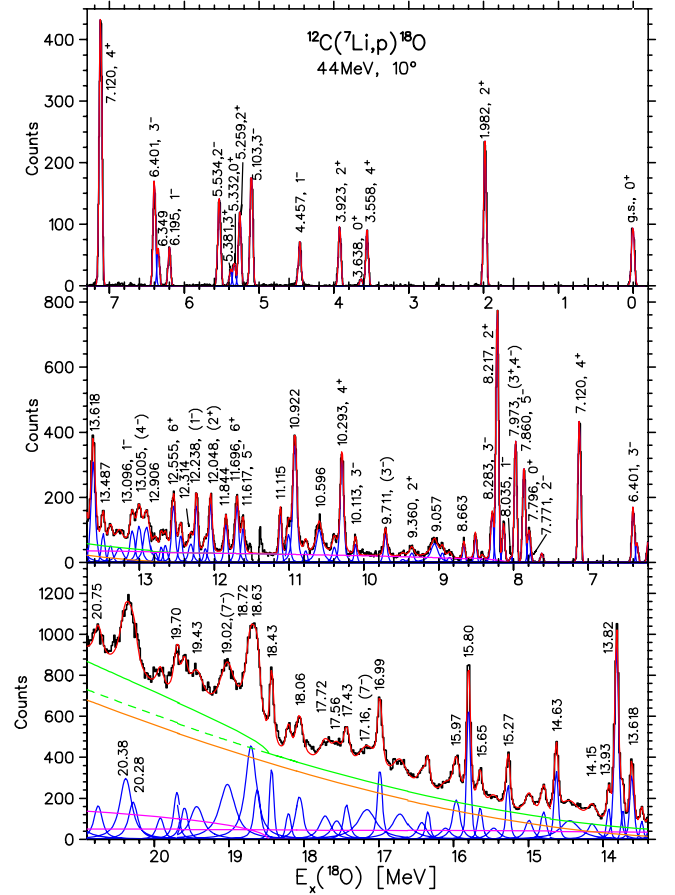


**Fig. 3.** (Color online) Energy spectrum of protons obtained with the Q3D spectrometer for the reaction  ${}^7\text{Li} + {}^{12}\text{C} \rightarrow \text{p} + {}^{18}\text{O}$  measured at 44.0 MeV incident energy and  $\theta_{lab} = 10^\circ$ . The lines are explained in the text (sect. 2.1).

of 98.9%. To determine contributions from oxygen in the  ${}^{12}\text{C}$  target, a  $\text{V}_2\text{O}_5$  target of  $69 \mu\text{g}/\text{cm}^2$  on a  ${}^{12}\text{C}$  backing of  $20 \mu\text{g}/\text{cm}^2$  was used. Only negligible contributions from oxygen ( $< 1\%$ ) and  ${}^{13}\text{C}$  (1.1% natural share) were observed in the spectra.

The measurements have been performed at three scattering angles  $\theta_{lab} = 10^\circ, 20^\circ$  and  $39^\circ$ . The solid angle was  $13.85 \text{ msr}$  (horizontal opening:  $6^\circ$ ). Ten (10) field settings (with regions of overlap of about 10%) were needed per angular setting in order to cover an excitation energy range of 21 MeV. The resulting 10 spectra were joined together and normalized in the overlapping regions. With an energy resolution from the beam of 5 keV, the final resolution of 45 keV achieved is mainly due to the energy loss differences in the target between projectile and ejectile. This resolution becomes worse at the larger angles due to larger values of the kinematical factor, which influences the final width due a limiting value of the beam emittance. The  ${}^{18}\text{O}$  spectrum at  $\theta_{lab} = 10^\circ$  is shown in fig. 3 and for  $\theta_{lab} = 39^\circ$  in fig. 4. Strong and rather narrow lines are observed well above the particle thresholds for  $\alpha$  and neutron emission at 6.226 MeV and 8.044 MeV, respectively. The particle thresholds for  ${}^{18}\text{O}$  are listed in table 1.

<sup>1</sup> Application Specific Integrated Circuit.

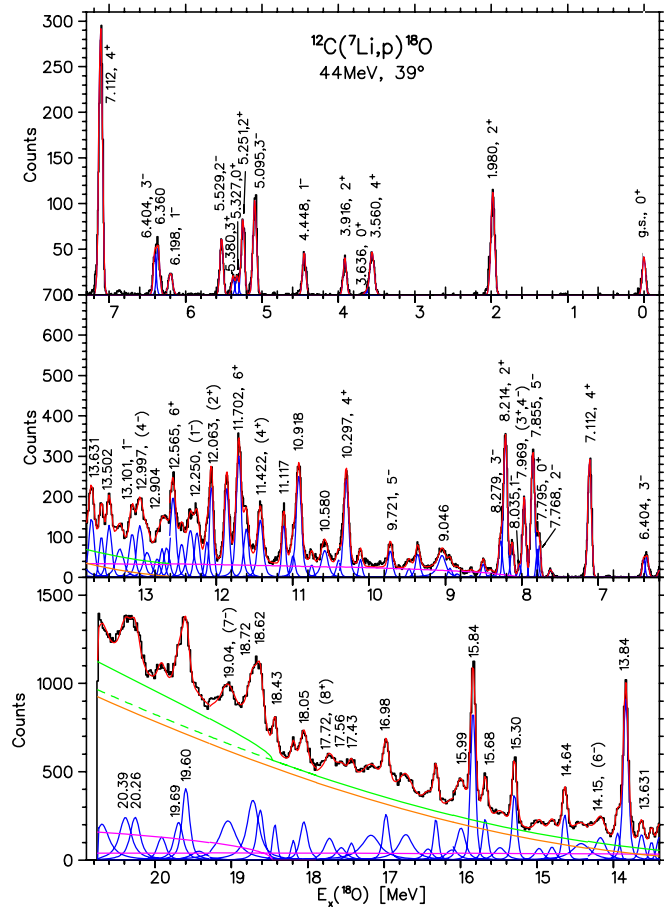


**Fig. 4.** (Color online) Energy spectrum of protons obtained with the Q3D spectrometer for the reaction  ${}^7\text{Li} + {}^{12}\text{C} \rightarrow \text{p} + {}^{18}\text{O}$  at  $\theta_{lab} = 39^\circ$ . The lines are explained in the text (sect. 2.1).

**Table 1.** Particle thresholds for  ${}^{18}\text{O}$ .

$S_\alpha$ [MeV]	$S_n$ [MeV]	$S_{2n}$ [MeV]	$S_p$ [MeV]
6.226	8.044	12.187	15.942

In the analysis of the spectra the lines in the particle-stable region have been fitted using Gaussians, and above particle thresholds with Breit-Wigner line shapes, their intrinsic width has been obtained using the fitting code SPEC [28]. The large number of narrow states at higher excitation energies points to their particular structure and to potentially high spins. The energy calibration was obtained with the positions of the sharp well-known levels [6] in  ${}^{18}\text{O}$  below 10 MeV, the overall agreement up to 11 MeV excitation energy was found to be within 5 keV. In this analysis 96 states were identified, 30 of these are new.

In the spectra there is almost no background from target contaminants. At higher excitation energies, however, continua of two 3-body distributions and one 4-body distribution appear, starting at the corresponding thresholds. The flat backgrounds in figs. 3, 4 correspond to the 3-body phase-space distributions for the three particles: i)  $n + {}^{17}\text{O}_{gs}$  (both not detected) and  $p$  (detected), and ii)  $p + {}^{17}\text{N}^*$  (both not detected) and  $p$  (detected).

**Table 2.** Experimental excitation energies between 7.0 MeV und 8.5 MeV in  ${}^{18}\text{O}$ , measured at  $\theta_{lab} = 10^\circ$ , and the corresponding literature values from ref. [6].

$J_{Lit}^\pi$	$E_{x,Lit}$ [MeV]	$E_x(10^\circ)$ [MeV]	$E_x - E_{x,Lit}$ [keV]
$4^+$	7.117(1)	7.120(3)	3
$1^-$	7.616(1)	7.619(5)	5
$2^-$	7.771(1)	7.792(4)	21
$5^-$	7.864(5)	7.860(4)	-4
$(3^+, 4^-)$	7.977(4)	7.973(3)	-4
$1^-$	8.038(1)	8.035(4)	-3
$5^-$	8.125(2)	8.130(4)	5
$2^+$	8.213(4)	8.217(4)	4
$3^-$	8.282(3)	8.283(5)	1
$(2^-)$	8.410(8)	8.414(5)	4

At about 12.8 MeV the 4-body phase-space distribution ( $n + n + {}^{16}\text{O}_{gs} + p$ ) (orange line) becomes visible. The correct description of the background shapes is quite important. These functions are calculated in the code SPEC [28]. The green continuous lines in figs. 3, 4 represent the sum of all phase-space distributions.

The spectra at  $10^\circ$  (fig. 3),  $20^\circ$  (not shown) and  $39^\circ$  (fig. 4) have been analyzed in this way. In the overlap regions of the 10 individual sections of the spectra some states may be affected causing some systematic error at that place in the fits. However, with the other angles these overlaps occur at different regions of excitation energies, and thus these uncertainties can be eliminated.

Due to the careful calibrations and the high-energy resolution we investigated the excitation energy region between 7.5 MeV and 8.4 MeV with the aim to search for previously unresolved states. Table 2 shows the fitted peak positions at  $10^\circ$  in comparison to the excitation energies from the literature [6]. The values all agree within  $\pm 5$  keV in their absolute value to the known excitation energies, except the  $2^-$  state at 7.792 MeV. Its fitted position has a too large deviation (21 keV). We can determine peak positions with a 5 keV uncertainty due to the good statistics (and 45 KeV of the resolution), and postulate that there is a doublet at 7.792 MeV. Therefore we unfolded this peak with two states: the  $J^\pi = 2^-$  state at its literature value 7.771(5) MeV and a new state, which we find at 7.796(5) MeV. The same value within 5 keV is found in the fits (using the program SPEC [28]) of the other two spectra. Figure 5 shows in an expanded scale the region between 7.5 MeV and 8.35 MeV excitation energy at the angles of  $10^\circ$ ,  $20^\circ$  and  $39^\circ$ . The 7.796 MeV state clearly dominates at  $10^\circ$ , whereas two states are definitely needed at larger angles to obtain an optimum fit to the energy spectrum. This new state is a very good candidate for the “missing” band head of the molecular band as discussed later (sect. 4.4 and fig. 10).

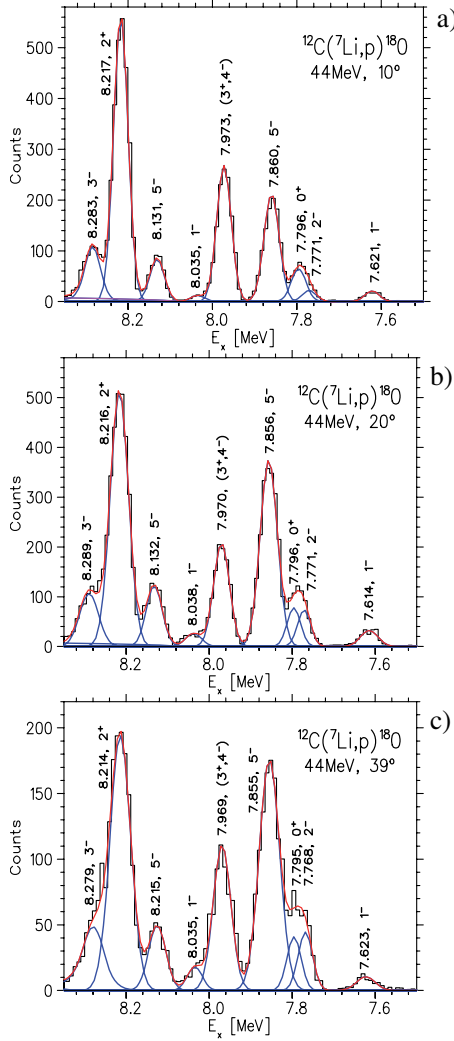


**Fig. 5.** (Color online) Regions of  $^{18}\text{O}$  spectra near 8 MeV at (a)  $10^\circ$ , (b)  $20^\circ$  and (c)  $39^\circ$ , showing a doublet at 7.8 MeV and the determination of the 7.796 MeV ( $J^\pi = (0^+)$ ) state.

### 3 Discussion of cluster bands

#### 3.1 Shell model and cluster structure

The different structures of the  $^{18}\text{O}$  nucleus can be characterized by the configurations (see fig. 1): i)  $^{16}\text{O} \otimes 2n$ , ii)  $^{14}\text{C} \otimes \alpha$ , and iii)  $^{12}\text{C} \otimes 2n \otimes \alpha$ . All these structures can be populated in the  $^{12}\text{C}(^7\text{Li}, p)^{18}\text{O}$  reaction, which we have used in our investigations. In this case we transfer “ $^6\text{He}$ ” or rather an  $\alpha$ -particle and 2 neutrons to the  $^{12}\text{C}$  target in arbitrary sequence. The configuration  $^{16}\text{O} \otimes [\nu(sd)^2]$  is characterized by 2-particle–0-hole (2p-0h) configurations with even parity. Another possibility is a (2p-2h) proton excitation of the  $^{16}\text{O}$  core, which leads to (4p-2h) states with  $^{14}\text{C} \otimes [\pi(sd)^2 \otimes \nu(sd)^2]$  structures and with a strong parentage to the  $^{14}\text{C} \otimes \alpha$  cluster configuration. Furthermore, we expect the molecular  $^{12}\text{C} \otimes 2n \otimes \alpha$  structure consisting of a  $^{12}\text{C}$  core and an  $\alpha$ -particle, bound by two valence neutrons. In a shell model description this corresponds to a (6p-4h) configuration with 2 pro-

**Table 3.** Components of wave functions for the first three  $0^+$  and  $2^+$  states and for the first two  $4^+$  states in  $^{18}\text{O}$  (dataset “constrained II” from Lawson *et al.* [19] and Sherr *et al.* [29]).

		Configurations		
$J^\pi$	$E_x$ [MeV]	$\nu(d_{5/2})^2$	$\nu(s_{1/2})^2$	coll.
$0_1^+$	0.00	<b>0.719</b>	0.192	0.088
$0_2^+$	3.63	0.213	0.112	<b>0.676</b>
$0_3^+$	5.33	0.068	<b>0.696</b>	0.236
$J^\pi$	$E_x$ [MeV]	$\nu(d_{5/2})^2$	$\nu(d_{5/2}, s_{1/2})$	coll.
$2_1^+$	1.98	<b>0.599</b>	0.235	0.120
$2_2^+$	3.92	<b>0.381</b>	<b>0.366</b>	0.251
$2_3^+$	5.26	0.002	0.362	<b>0.629</b>
$J^\pi$	$E_x$ [MeV]	$\nu(d_{5/2})^2$	$\nu(d_{5/2}, d_{3/2})$	coll.
$4_1^+$	3.56	<b>0.972</b>	0.023	0.004
$4_2^+$	7.11	0.014	0.154	<b>0.832</b>

tons and 4 neutrons in the ( $sd$ ) shell corresponding to a  $^{12}\text{C} \otimes [\pi(sd)^2 \otimes \nu(sd)^2]_\alpha \otimes \nu(2s1d)^2$  structure. An odd-particle–odd-hole excitation produces odd-parity states by excitations from the ( $1p$ ) shell to the ( $2s1d$ ) shell. However, the rotational bands of negative parity, which represent the parity inversion partners due to the underlying cluster structure, need higher order  $xp$ - $yh$  excitations and thus are very difficult to obtain in shell model calculations.

The microscopic structure of the low-lying states in  $^{18}\text{O}$  is understood on the basis of the analysis of Lawson *et al.* [19] (table 3). The major components of the wave function for all positive-parity states below 7.2 MeV arise from the ( $2s1d$ ) model space. There is also one core-excited collective state for each of the spins  $0^+$ ,  $2^+$  and  $4^+$ . Those states, which have a predominantly collective structure and thus strong configuration mixing (though they are predominantly of (4p-2h) configuration), are the states at  $E_x = 3.63$  MeV, 5.26 MeV and 7.11 MeV [19] as marked in the last column in table 3.

#### 3.2 Parity splitting of rotational cluster bands

The cluster and molecular structures studied in the present work consist of two different clusters with different size (for example  $^{14}\text{C} \otimes \alpha$ ). Such cluster structures usually correspond to octupole deformations of the nucleus, which leads to specific properties of the rotational bands. In the book of Herzberg [30] the nature of the rotational spectra of molecular structures is reviewed. The most important aspect for an intrinsically asymmetric structure is the broken intrinsic reflection symmetry. Such systems have no well-defined parity. The parity projection, which is obtained from the linear combinations of two reflected states using a positive and a negative sign, respectively, leads to a splitting of the rotational bands. The feature of symmetry breaking has been explored in nuclear physics by Bohr and Mottelson [31], where this phenomenon appears with the odd multipoles of deformation, in particular with the octupole deformation [31–34].

For reflection-asymmetric but axial-symmetric systems the signs in the linear combinations correspond to the *signature*  $r$  defined as the eigenvalues of the  $R$  operator.  $R$  describes a rotation of  $180^\circ$  about an axis perpendicular to the symmetry axis [31,32]:

$$r = e^{-i\pi J}. \quad (1)$$

Here  $J$  is the spin and  $\pi$  the intrinsic parity. For systems with intrinsic octupole-deformed shapes and an even number of nucleons a parity doublet appears [33] with bands for  $r = \pm 1$  and an energy splitting between them:

$$r = +1, \quad J^\pi = 0^+, 2^+, 4^+, \dots, \quad (2)$$

$$r = -1, \quad J^\pi = 1^-, 3^-, 5^-, \dots \quad (3)$$

This feature allows clear predictions for the states. Their properties of broken symmetry gives rise to the splitting of the rotational bands into the parity inversion doublet.

We can therefore identify for the nuclear molecules, formed with two clusters of different size, two rotational bands (the parity inversion doublet), which originate from the same intrinsic structure. For the  $^{14}\text{C} \otimes \alpha$  cluster configuration in  $^{18}\text{O}$  with  $\phi_r = |^{14}\text{C} \otimes \alpha\rangle$  ( $\alpha$ -cluster right),  $\phi_l = |\alpha \otimes ^{14}\text{C}\rangle$  ( $\alpha$ -cluster left), and  $N$  as a normalisation factor, the linear combination can be written as follows:

$$\Phi^\pm = N(\phi_r \pm \phi_l).$$

The wave functions  $\Phi^+$  and  $\Phi^-$

$$|\Phi^\pm\rangle = \frac{1}{\sqrt{2(1 \pm \langle \phi_r | \phi_l \rangle)}} (|\phi_r\rangle \pm |\phi_l\rangle) \quad (4)$$

have eigenvalues

$$E^\pm = \frac{1}{(1 \pm \Delta)} (\bar{E} \pm E_\Delta) \quad (5)$$

with  $\Delta = \langle \phi_r | \phi_l \rangle$  the non-orthogonality,  $\bar{E} = 1/2(E_r + E_l)$  and  $E_\Delta = \langle \phi_r | H | \phi_l \rangle$ . For  $\Delta \ll 1$ , we have in first order the following energies:

$$E^\pm \approx \bar{E} \pm \delta_E \quad (6)$$

with

$$\delta_E = E_\Delta - \bar{E} \cdot \Delta. \quad (7)$$

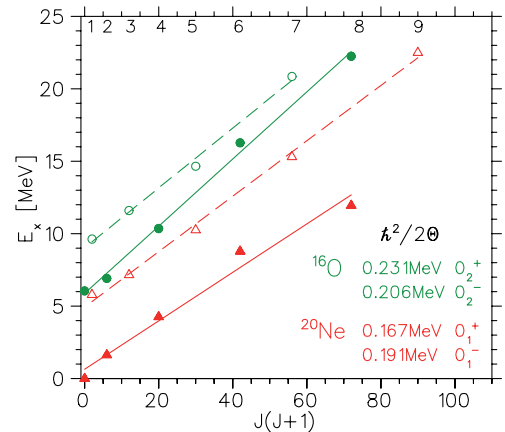
The energy splitting amounts to  $E^+ - E^- = 2 \cdot \delta_E$  (see eq. (6)). The value of this energy splitting reflects the intrinsic asymmetric structure.

Figure 6 illustrates the splitting of the known parity doublet bands for the  $\alpha$ -cluster structures  $^{12}\text{C} \otimes \alpha$  of  $^{16}\text{O}$  and for  $^{16}\text{O} \otimes \alpha$  of  $^{20}\text{Ne}$ . We will come back to these structures in connection with the discussion of  $^{18}\text{O}$  in sect. 4.3.

## 4 Results for rotational bands in $^{18}\text{O}$

The excitation energy  $E_x$  of the members of a rotational band depends on the total angular momentum  $J$  as follows [31]:

$$E_x(J) = \frac{\hbar^2}{2\Theta} [J(J+1)] + E_0. \quad (8)$$



**Fig. 6.** (Color online) The  $\alpha$ -cluster bands of positive (solid lines) and negative (dashed lines) parity in  $^{16}\text{O}$  [35] (green filled and open circles, respectively) in comparison with these structures in  $^{20}\text{Ne}$  [36] (red filled and open triangles, respectively). The lines represent linear fits through the experimental data, numbers correspond to the fitted slope parameters (see eq. (8)).

**Table 4.** Members of the  $K^\pi = 0_1^+$  ground-state band in  $^{18}\text{O}$ . The following entries are shown: spins and parities  $J^\pi$ , excitation energies  $E_x$ , cross-sections  $d\sigma/d\Omega$  in the centre-of-mass system at  $\theta_{lab} = 10^\circ$  and results from the literature [6].

$J^\pi$	$E_x$ [MeV]	$(d\sigma/d\Omega)_{cm}$ [ $\mu\text{b}/\text{sr}$ ] $\theta_{lab} = 10^\circ$	$J_{Lit}^\pi$	$E_{x,Lit}$ [MeV]
$0^+$	0.000(4)	2.82(17)	$0^+$	0.000
$2^+$	1.982(4)	6.31(25)	$2^+$	1.982
$4^+$	3.558(5)	2.35(11)	$4^+$	3.555

Here the factor  $\hbar^2/2\Theta$  (unit: [MeV]) is the *slope parameter* obtained in a linear fit between  $E_x(J)$  and  $J(J+1)$ , where  $\Theta$  is the moment of inertia with respect to the rotational axis of the deformed nucleus in the given cluster configuration, and  $E_0$  is the constant obtained in the fit.

We present here results for bands, where some members are already known. We are able to extend these by further band members and identify also the corresponding negative-parity bands of the inversion doublets. To establish the bands we used several informations: i) the relation between  $E_x$  and  $J$  (eq. (8)), ii) the  $(2J+1)$ -dependence of cross-sections and their angular dependences, iii) information from the AMD calculations, as well as GCM calculations. Tentative assignments for all members of the rotational bands have been made in this way.

### 4.1 $K^\pi = 0_1^+$ ground-state band

All members of the well-known ground-state band of  $^{18}\text{O}$  are observed [8]:  $0^+$  at 0.00 MeV,  $2^+$  at 1.98 MeV and  $4^+$  at 3.56 MeV (table 4). These states are characterized by the  $^{16}\text{O} \otimes 2n$  configuration with the  $^{16}\text{O} \otimes [\nu(d_{5/2})^2]$  structure (see table 3), they do not form a rotational band.

**Table 5.** Members of the positive-parity  $K^\pi = 0_2^+$  cluster band in  $^{18}\text{O}$ : spins and parities  $J^\pi$ , excitation energies  $E_x$ , widths of resonances  $\Gamma$ , cross-sections  $d\sigma/d\Omega$  at  $\theta_{lab} = 10^\circ$  (see also fig. 7) and results from the literature [6].

$J^\pi$	$E_x$ [MeV]	$\Gamma$ [keV]	$(d\sigma/d\Omega)_{cm}$ [ $\mu\text{b}/\text{sr}$ ] $\theta_{lab} = 10^\circ$	$J_{Lit}^\pi$	$E_{x,Lit}$ [MeV]
$0^+$	3.638(5)		0.28(5)	$0^+$	3.634
$2^+$	5.259(4)		3.21(13)	$2^+$	5.255
$4^+$	7.120(4)	< 10	12.06(30)	$4^+$	7.117
$6^+$	11.696(6)	19(7)		$6^+$	11.69
$(8^+)$	18.062(15)	80(15)	19.35(31)		18.049

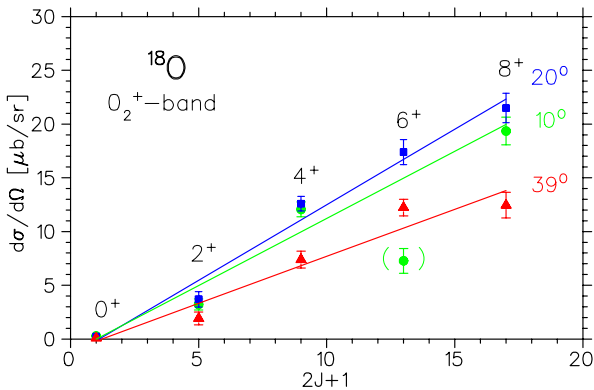


**Fig. 7.** (Color online) Differential cross-sections for members of the  $K^\pi = 0_2^+$  rotational cluster band in  $^{18}\text{O}$ , for different reaction angles, plotted as a function of spin ( $2J + 1$ ).

The structure terminates at the expected maximum spin value  $J^\pi = 4^+$ .

#### 4.2 The $K^\pi = 0_2^+$ cluster band

In this section we discuss the results for the  $^{18}\text{O}$  rotational band based on the  $K^\pi = 0_2^+$  state at 3.64 MeV. The first four members of this (4p-2h) cluster rotational band corresponding to the  $^{14}\text{C} \otimes \alpha$  intrinsic structure in  $^{18}\text{O}$  are well established [9, 10, 16, 19, 22, 23]. We observed this positive-parity cluster band with the  $0_2^+$  band head at 3.64 MeV, the  $2_3^+$  member at 5.56 MeV, the  $4_2^+$  at 7.11 MeV and the  $6_1^+$  at 11.69 MeV. The  $(8^+)$  state was proposed by Cunsolo *et al.* [10] at  $(17.6 \pm 0.2)$  MeV as a fifth member of this band. We suggest that the  $(8^+)$  member is located at 18.06 MeV (see table 5), because this state is well populated in the present  $^{12}\text{C}(^7\text{Li}, p)$  reaction (figs. 3, 4) and also in the  $^{14}\text{C}(^6\text{Li}, d)$  reaction of Cunsolo *et al.* [10] (see there fig. 1b), where this relatively narrow state at 18.1 MeV has not been further considered. The energy of the 18.06 MeV  $(8^+)$  state is consistent with the  $J(J+1)$  rule (see eq. (8) and fig. 8) and the differential cross-sections follow well the  $(2J+1)$  systematics (fig. 7). These systematics are obtained at the three measured angles (at  $10^\circ$  the value for the  $6^+$  state just falls to the edge of the overlapping partial spectra and is therefore not given in table 5).

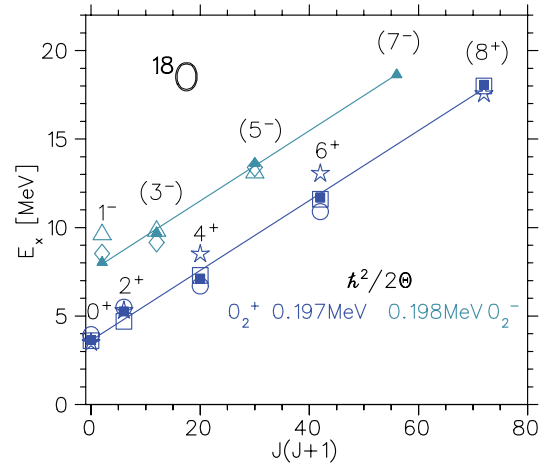


**Fig. 8.** (Color online) Energy systematics for the members of the  $^{18}\text{O}$   $\alpha$ -cluster rotational parity doublet with  $K^\pi = 0_2^+$  (filled squares) and with  $K^\pi = 0_2^-$  (filled triangles) as a function of  $J(J+1)$ . The values of fitted slope parameters (see eq. (8)) are indicated. Results from theoretical calculations are also displayed: GCM calculations [22] by open squares ( $K^\pi = 0_2^+$ ), and open triangles ( $K^\pi = 0_2^-$ ); AMD+GCM calculations [23] by open circles ( $K^\pi = 0_2^+$ ), and open diamonds ( $K^\pi = 0_2^-$ ) shifted by  $-4.6$  MeV; shell model calculations (see sect. 4.2) by open stars ( $K^\pi = 0_2^+$ ).

In the theoretical work of Buck *et al.* in the framework of the  $\alpha$ -cluster folding model [37] the authors obtain the  $(8^+)$  state at 18.03 MeV, and in the work of Descouvemont and Baye [22] in the framework of the Generator Coordinate Method (GCM) the  $(8^+)$  state is obtained at 18.0 MeV, with a resonance width of 100 keV. These results support our choice that the  $(8^+)$  state at  $E_x = 18.06$  MeV is the fifth member of the  $K^\pi = 0_2^+$  positive-parity cluster band.

Further theoretical calculations have been used to support the selection of the members of the  $K^\pi = 0_2^+$  cluster band. We performed for this band shell model calculation using the code OXBASH [38] with the “*psdprn*” model space and the single-particle energies and with the “*psdmwkpri*” interaction [39]. For the members of the (4p-2h) cluster band corresponding to the  $^{14}\text{C} \otimes \alpha$  intrinsic structure we have selected those theoretical states, which have  $\pi(2p-2h)$  proton excitations  $\pi[(1p)^{-2}(2s1d)^2] \otimes \nu(2s1d)^2$  and which possess a good collectivity. Our shell model calculations are in agreement with the experimental data (see open stars in fig. 8). The (AMD+GCM) theoretical calculations by Furutachi *et al.* [23] also reproduce the members of the  $K^\pi = 0_2^+$  cluster band with a common shift of  $-4.6$  MeV (open circles in fig. 8). The band head is experimentally located at an excitation energy 2.58 MeV below the  $\alpha$ -cluster threshold.

#### 4.3 $K^\pi = 0_2^-$ cluster band

In order to establish the inversion partner of negative parity we use several points for its identification. To determine the energy splitting  $2\delta_E$  (eq. (6)) between the  $K^\pi = 0_2^\pm$

**Table 6.** Members of the negative-parity  $K^\pi = 0_2^-$  cluster band in  $^{18}\text{O}$ . In the first four columns the following entries are shown: spins and parities  $J^\pi$ , excitation energies  $E_x$ , widths of resonances  $\Gamma$  and cross-sections  $d\sigma/d\Omega$  in the centre-of-mass system of the present measurement. The next two columns show results from  $\alpha$ - $^{14}\text{C}$  angular-correlation studies in the decay of  $^{18}\text{O}$  [15,40]. In the last two columns are given spins and parities  $J^\pi$ , and excitation energies  $E_x$  from the literature [6].

$J^\pi$	$E_x$ [MeV]	$\Gamma$ [keV]	$\left(\frac{d\sigma}{d\Omega}\right)_{cm}$ [ $\mu\text{b}/\text{sr}$ ] $\theta_{lab} = 10^\circ$	$E_x$ [MeV] $^{14}\text{C}(^{18}\text{O}; \alpha, ^{14}\text{C})$ [15]	$E_x$ [MeV] $^9\text{Be}(^{18}\text{O}; \alpha, ^{14}\text{C})$ [40]	$J_{Lit}^\pi$	$E_{x,Lit}$ [MeV]
$1^-$	8.035(5)	< 10	0.43(8)	8.04 ( $1^-$ )		$1^-$	8.038
$(3^-)$	9.711(4)	15(4)	3.26(13)	9.70 ( $(3^-)$ )	9.72 ( $(3^-)$ )	$(5^-)$	9.713
$(5^-)$	13.624(8)	22(7)	16.32(35)				
$(7^-)$	18.63(1)	100(20)	29.92(64)				

parity doublet bands, we compare the  $^{14}\text{C} \otimes \alpha$  structure in  $^{18}\text{O}$  with the well-established  $^{12}\text{C} \otimes \alpha$  structure in  $^{16}\text{O}$  ( $K^\pi = 0_2^\pm$ ) [35] and the  $^{16}\text{O} \otimes \alpha$  structure in  $^{20}\text{Ne}$  ( $K^\pi = 0_1^\pm$ ) [36] (fig. 6). For these neighboring nuclei the parity doublet energy splitting is approximately 2.9 MeV and 4.8 MeV, respectively. In the framework of the Weak Coupling Model (WCM) we then expect an energy splitting  $2\delta_E$  for the cluster parity doublet in  $^{18}\text{O}$  of about 3.85 MeV. Therefore the  $1^-$  band head of the  $E_x(0_2^-)$  band is expected close to  $E_x(0_2^+) + 2\delta_E + 0.2(J(J+1)) = 3.64 + 3.85 + 0.40$  (for  $J = 1$ ) MeV  $\approx 7.9$  MeV (using 0.2 MeV for the slope parameter, see fig. 8). We have localized this band head as a well-known  $1^-$  state at 8.035(5) MeV (see table 6). This state was also observed in the  $^{14}\text{C}(^{18}\text{O}; \alpha, ^{14}\text{C})^{14}\text{C}$  reaction by Curtis *et al.* [15]. In their work the  $\alpha$ -cluster structure in  $^{18}\text{O}$  was investigated using a  $^{14}\text{C} + \alpha$  angular-correlation measurement technique. Therefore we suggest, that this  $1^-$  state is an  $\alpha$ -cluster state and is the band head of the  $K^\pi = 0_2^-$  cluster band with the intrinsic  $^{14}\text{C} \otimes \alpha$  configuration. The energy of the parity splitting is almost identical to the value in  $^{20}\text{Ne}$ , indicating a similar role of the clusters  $^{14}\text{C}$  and  $^{16}\text{O}$ .

The members of the rotational band built on the  $1^-$  state at 8.04 MeV have been observed in the present work up to  $J^\pi = (7^-)$ . The second member is the  $3^-$  state at 9.71 MeV, which was also determined as a  $J^\pi = (3^-)$  state in the works of Cunsolo *et al.* [9], Ashwood *et al.* [40] (cf. table 6) and Goldberg *et al.* [18]. Furthermore we propose for the state at 13.624 MeV a spin and parity  $(5^-)$  and for the state at 18.632 MeV  $(7^-)$ , which both form further members of the  $K^\pi = 0_2^-$  band in  $^{18}\text{O}$  as discussed below. Our energy splitting for this  $K^\pi = 0_2^\pm$  doublet of about 4.0 MeV is in good agreement with results of Descouvemont and Baye [22] and of Furutachi *et al.* [23] (4.2 MeV). Note that the energy splitting is calculated always as the energy distance between the two lines of the doublet bands at the same  $J$ -value, not as the energy difference for the  $0^+$  and the  $1^-$  band heads.

In our shell model calculations we can not find states corresponding to the members of the negative-parity band, because they correspond to excitations into the  $(1f2p)$ -shell. The GCM-calculations of Descouvemont and Baye [22] (open triangles in fig. 8) and the (AMD+GCM)

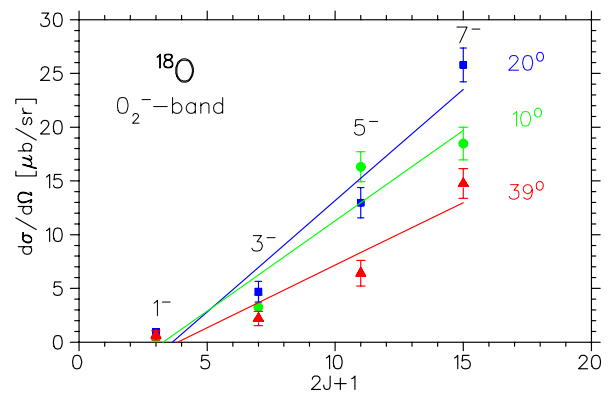


**Fig. 9.** (Color online) Differential cross-sections for members of the  $K^\pi = 0_2^-$  rotational cluster band in  $^{18}\text{O}$ , for different reaction angles, plotted as a function of spin  $(2J+1)$ .

calculations by Furutachi *et al.* [23] (open diamonds in fig. 8 shown with a common shift of  $-4.6$  MeV) reproduce very well the proposed members of the  $K^\pi = 0_2^-$  negative-parity partner of the inversion doublet.

Also the systematics of differential cross-sections as a function of spin  $J$  for the members of the negative-parity band follows quite well a linear dependence on  $(2J+1)$ , as shown in fig. 9.

#### 4.4 $K^\pi = 0_4^+$ and $K^\pi = 0_4^-$ molecular bands

For the molecular band, which has an intrinsic structure  $^{12}\text{C} \otimes 2n \otimes \alpha$ , the three known members  $2^+$ , 8.216 MeV,  $4^+$ , 10.293 MeV, and  $6^+$ , 12.55 MeV [8,15] are also observed in the present work. The  $0^+$  band head, suggested by Fortune at 7.11 MeV [8], has now been identified for the first time as the  $0_4^+$  state at 7.796(5) MeV (see sect. 2). Furthermore, using the  $J(J+1)$  rule for the excitation energy and taking into account that the states of this molecular band should be strongly populated in our  $(^7\text{Li}, p)$ -reaction with a  $(2n \otimes \alpha)$  transfer, we extended this band by tentatively assigning states  $J^\pi = (8^+)$  at 15.81 MeV and  $(10^+)$  at 20.38 MeV. GCM calculations by Descouvemont and Baye [22] (open diamonds in fig. 10) reproduce well the

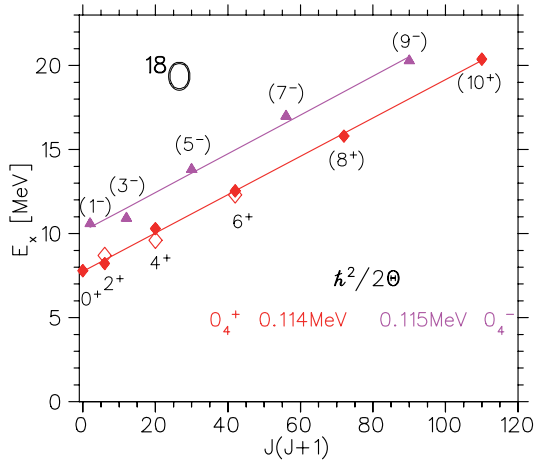


**Fig. 10.** (Color online) Energy systematics for the members of the  $K^\pi = 0_4^\pm$  molecular rotational bands of  $^{18}\text{O}$  forming a parity inversion doublet based on the  $0_4^+$  band head at 7.796(5) MeV as a function of  $J(J+1)$ . The slope parameters for both rotational bands are indicated. The open diamonds show results of GCM calculations [22] with a shift of  $-2.0$  MeV.

three known members of this  $K^\pi = 0_4^+$  molecular band with a common shift of  $-2.0$  MeV.

The  $^{12}\text{C} \otimes 2n \otimes \alpha$  structure (fig. 1) is an intrinsic reflection asymmetric configuration, thus we expect also here a parity inversion doublet. As in the case of the positive-parity band, the states of the negative-parity molecular band should be strongly populated in the  $(^7\text{Li}, p)$ -reaction. We suggest for the first five members of the negative-parity partner the states: 10.59 MeV ( $(1^-)$ ), 10.92 MeV ( $(3^-)$ ), 13.82 MeV ( $(5^-)$ ), 16.99 MeV ( $(7^-)$ ) and 20.28 MeV ( $(9^-)$ ) MeV), where the tentative spin assignments were obtained using the  $J(J+1)$  systematics for the excitation energies (see table 7 and fig. 10). The energy splitting for the  $K^\pi = 0_4^\pm$  molecular inversion doublet is 2.4 MeV. The smaller value in comparison to the  $K^\pi = 0_2^\pm$  cluster inversion doublet (4.0 MeV) shows, that the molecular configuration has a larger deformation and a larger spatial dimension making the non-orthogonality overlap smaller. The energy splitting between positive- and negative-parity states becomes smaller, when the overlap integral between the direct and reflected intrinsic shape  $\langle \phi_r | \phi_l \rangle$  is smaller. This is expected, when the distance between the two clusters is larger (see sect. 3.2). We must assume that in the covalent binding picture the neutrons are in  $\pi$ -orbits, where the residual interaction between the two neutrons is large, similar to the  $^{10}\text{Be}$  ground state, where the extra binding energy is more than 8 MeV. Covalent configurations with  $\sigma$ -orbits would lead to an almost vanishing energy splitting.

#### 4.5 $K^\pi = 1^-$ band

In addition to the ground-state band and to the cluster inversion doublet bands described above, a negative-parity configuration band with a one-proton excitation based on the 4.457 MeV ( $J^\pi = 1_1^-$ ) state is proposed. The first three

**Table 7.** Members of the positive-parity  $K^\pi = 0_4^+$  (upper part) and negative-parity  $K^\pi = 0_4^-$  (lower part) molecular bands in  $^{18}\text{O}$ . In the first four columns the following entries are shown: spins and parities  $J^\pi$ , excitation energies  $E_x$ , widths of resonances  $\Gamma$ , and the cross-sections  $d\sigma/d\Omega$  in the centre-of-mass system of the present measurement. In the last column are given known excitation energies  $E_x$  from the literature [6].

$J^\pi$	$E_x$ [MeV]	$\Gamma$ [keV]	$(d\sigma/d\Omega)_{cm}$ [ $\mu\text{b}/\text{sr}$ ] $\theta_{lab} = 10^\circ$	$E_{x,Lit}$ [MeV]
$0^+$	7.796(5)	< 10	2.38(10)	[6, 8]
$2^+$	8.216(4)	< 10	20.25(45)	8.21
$4^+$	10.293(4)	23(8)	12.97(33)	10.29
$6^+$	12.557(6)	22(8)	7.67(16)	12.53
$(8^+)$	15.810(10)	20(8)	31.40(48)	
$(10^+)$	20.385(15)	155(25)	45.07(61)	
$(1^-)$	10.59(1)	70(16)	7.86(16)	[6]
$(3^-)$	10.92(1)	30(9)	17.26(41)	10.91
$(5^-)$	13.82(2)	27(8)	48.77(76)	
$(7^-)$	16.99(1)	50(12)	20.70(35)	
$(9^-)$	20.28(3)	120(21)	21.08(29)	

**Table 8.** Members of the negative-parity  $K^\pi = 1^-$  band in  $^{18}\text{O}$ . The following entries are shown: spins and parities  $J^\pi$ , excitation energies  $E_x$ , widths of resonances  $\Gamma$  and cross-sections  $d\sigma/d\Omega$  in the centre-of-mass system for the present measurement. In the last two columns are given: spins and parities  $J^\pi$  and excitation energies  $E_x$  from the literature [6].

$J^\pi$	$E_x$ [MeV]	$\Gamma$ [keV]	$(d\sigma/d\Omega)_{cm}$ [ $\mu\text{b}/\text{sr}$ ] $\theta_{lab} = 10^\circ$	$J_{Lit}^\pi$	$E_{x,Lit}$ [MeV]
$1^-$	4.457(5)		1.96(9)	$1^-$	4.456
$2^-$	5.534(4)		3.95(14)	$2^-$	5.530
$3^-$	8.283(5)	5(1)	4.34(18)	$3^-$	8.282
$(4^-)$	11.115(8)	5(5)	3.84(14)		11.13
$(5^-)$	14.63(1)	27(8)	16.94(32)		
$(6^-)$	18.43(1)	18(5)	15.16(29)		

members  $J^\pi = 1^-, 2^-$  and  $3^-$  of this  $K^\pi = 1^-$  band are known states with well-established spin assignments [6]. In order to identify higher-lying members we examined for possible candidates the systematics of excitation energies in dependence on  $J(J+1)$  by extrapolating the trend to  $J = 4$ ,  $J = 5$  and  $J = 6$ . Furthermore, we took into account that all states of this band have a very narrow width ( $< 30$  keV) and large cross-sections (see fig. 3 and table 8).

This  $K^\pi = 1_1^-$  band is shown in fig. 11 (filled triangles). Shell model calculations (open squares) performed with the shell model code OXBASH [38] describe the data quite well (with a common shift of  $-2.3$  MeV) using the  $(\pi[(1p_{1/2})^{-1}(sd)^1] \otimes \nu(sd)^2)$  ( $3p-1h$ ) configurations in  $^{18}\text{O}$ .

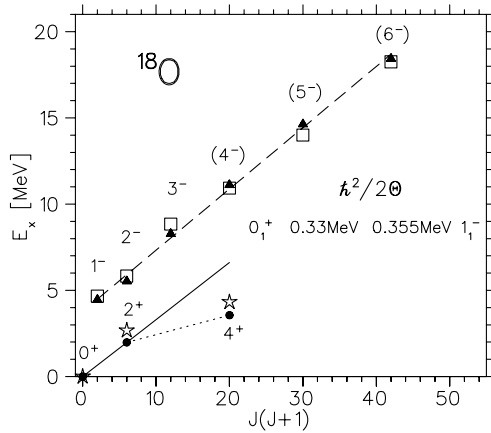


**Fig. 11.** Energies of the members of the  $K = 0_1^+$  ground-state band (filled circles) and  $K = 1^-$  one-proton excitation band (filled triangles) in  $^{18}\text{O}$  plotted as function of  $J(J+1)$ . A comparison with shell model calculations (open stars and squares) is shown (see text).

The  $K^\pi = 0_1^+$  ground-state band (filled circles), which is also well described by shell model calculations (open stars), is shown for comparison.

## 5 Reaction mechanisms

The reaction  $^7\text{Li} + ^{12}\text{C} \rightarrow \text{p} + ^{18}\text{O}$  has been studied previously at lower incident energy of 15–20 MeV [8, 14, 17].

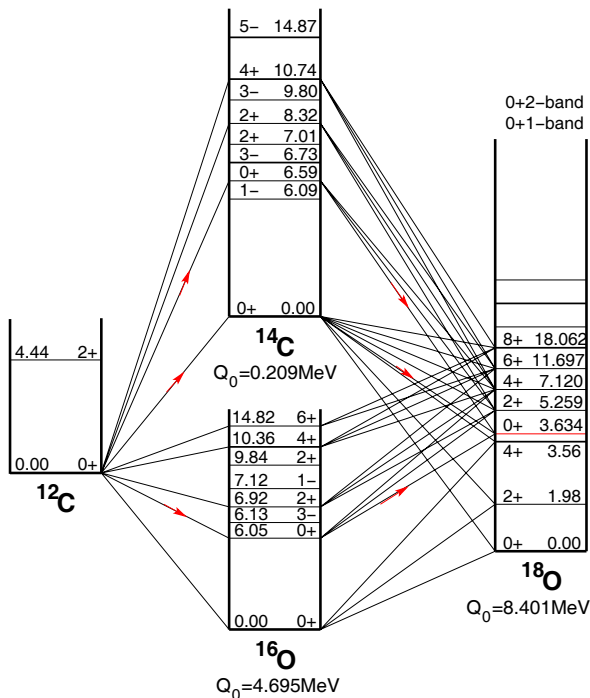


**Fig. 12.** (Color online) Coupling scheme for the sequential transfer of two neutrons and an  $\alpha$ -particle in either order to the final states of the  $^{18}\text{O}$  ground-state band and the  $K = 0_2^+$  band. The relevant intermediate states in  $^{14}\text{C}$  and  $^{16}\text{O}$  and also the  $Q$ -values are shown.

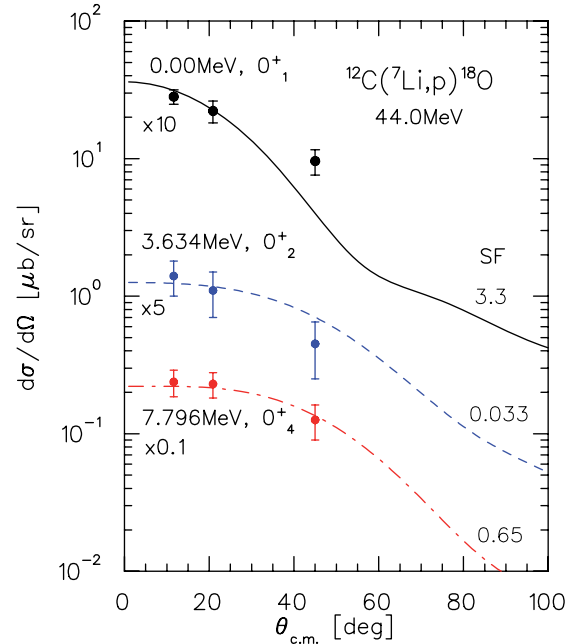


**Fig. 13.** (Color online) Angular distributions for the three  $0_1^+$  band heads of the  $^{18}\text{O}$  positive-parity bands discussed in the analysis. Lines correspond to FRESKO CRC calculations. The factors on the left are applied for the plot on a common scale.

In this case strong contributions from the compound nuclear-reaction mechanism were assumed. At the present energy of 44.0 MeV these contributions are expected to be smaller, and simultaneously the direct multi-nucleon transfer contributions are expected to be much stronger. Actually the angular distributions suggest a more direct mechanism, since for a compound decay a sharper rise towards smaller reaction angles should have been observed, in particular for higher spin values. The “ $^6\text{He}$ ” transfer has to be considered as a sequential transfer in two steps of two neutrons and an  $\alpha$ -particle in either order. We have specified for the two-step reaction calculations the dominant states populated in the intermediate steps in fig. 12, namely the two-neutron transfer on  $^{12}\text{C}$  to  $^{14}\text{C}$  (with subsequent  $\alpha$  transfer), and the  $\alpha$ -particle transfer on  $^{12}\text{C}$  to  $^{16}\text{O}$  (with subsequent 2n transfer). In these transfers a large variety of intermediate states in  $^{14}\text{C}$  and  $^{16}\text{O}$  must be considered.

Such calculations have been performed using the coupled reaction channel (CRC) code FRESKO [41]. It cannot be expected that absolute differential cross-sections can be obtained, because not all states will be included, and also microscopic amplitudes were not available. The coherent properties of the amplitudes being added in the calculations give in addition a dependence on the phases of different branches. However, the large number of transitions, which is explicitly taken into account, reduces the flux into a single exit channel. This has the effect to increase the mean absorption and the characteristic shapes of angular distributions for specific angular-momentum transfers are smoothed. We have therefore chosen for all spectroscopic amplitudes a value of 1.0, and have summarized the spectroscopic strength for the calculated transitions in a single

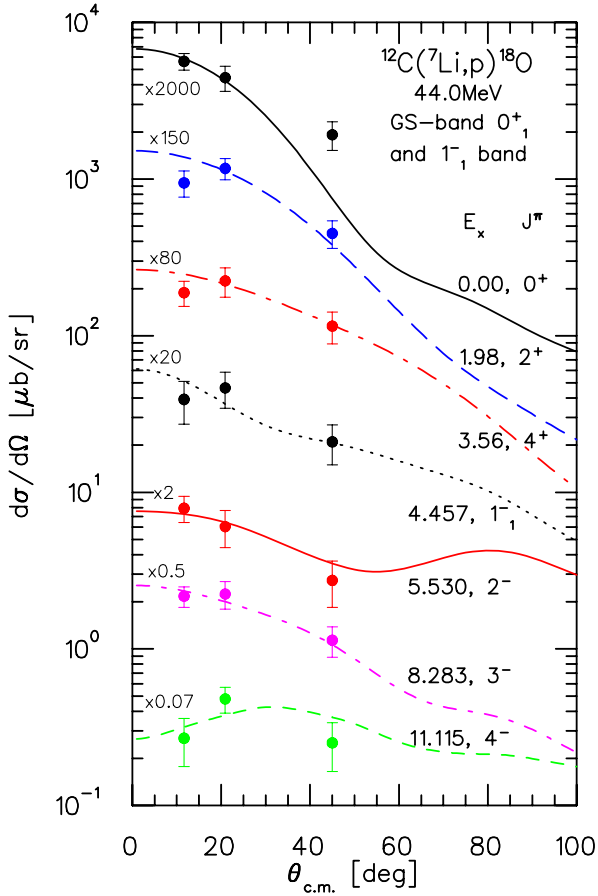


**Fig. 14.** (Color online) Angular distributions for the  $0_1^+$  ground-state band and the negative-parity  $K^\pi = 1_1^-$  band of  $^{18}\text{O}$ . The lines correspond to FRESKO CRC calculations. The factors on the left are applied for the plot on a common scale.

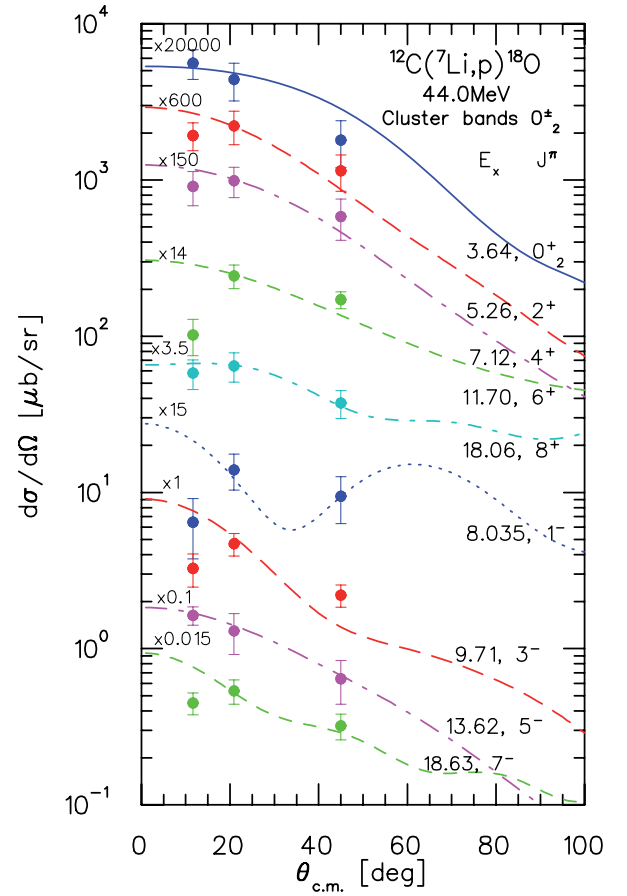


**Fig. 15.** (Color online) Angular distributions for the  $K^\pi = 0_2^\pm$  parity doublet bands of  $^{18}\text{O}$ . See also the caption of fig. 14 for more details.

strength factor “SF” to fit the absolute value of the cross-sections of the experimental angular distributions of  $^{18}\text{O}$  final states (see fig. 13). The shapes of the angular distributions still give some information in their dependence on spins and  $Q$ -values for the final states.

As discussed above, we have used for assignments of states the excitation energy systematics on the spin  $J$  in a plot of differential cross-sections as a function of  $(2J + 1)$  at the measured scattering angles. The proportionality to the spin factor  $(2J + 1)$  appears for both, the compound and the multi-nucleon transfer reaction mechanisms.

### 5.1 Angular distributions

Experimental angular distributions were obtained from the spectra taken at the three angles  $10^\circ$ ,  $20^\circ$  and  $39^\circ$  in the laboratory system. Comparison of these data with calculated angular distributions are given in figs. 13–16. In fig. 13 the shapes of the angular distributions for states with spin  $J^\pi = 0^+$  are compared. Clearly, a  $Q$ -value dependence of the shapes is observed, but besides this, no characteristic structures or differences between the shapes can be seen, also not in figs. 14–16. We note, however, that for higher spins the fall off to larger angles is weaker.

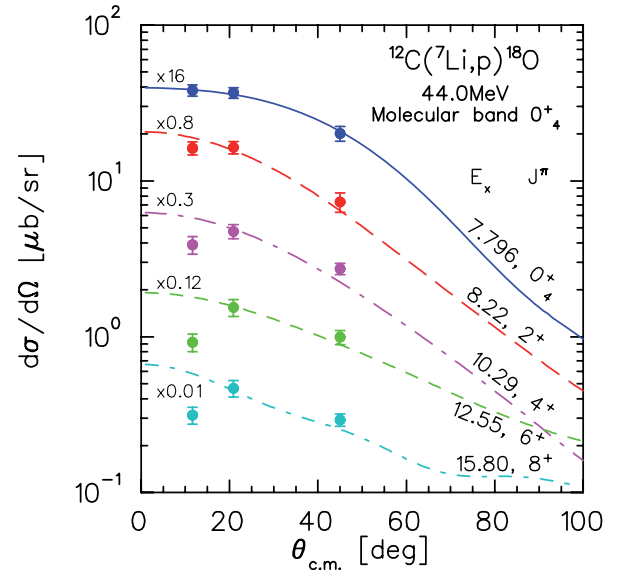


**Fig. 16.** (Color online) Angular distributions for the states of the  $K^\pi = 0_4^+$  molecular band in  $^{18}\text{O}$ . See also the caption of fig. 14 for more details.

## 6 Survey of all states

In this chapter we try to give a comprehensive overview of all theoretically expected states in comparison to the observation in the present experiment of the 96 states (30 are new) up to an excitation energy of 21 MeV. The reaction may still be selective in the population, and the resolution of 45 keV implies that above 10 MeV of excitation energy we may have missed a considerable number of states. With the described methods we have attempted to place the dominantly populated states into rotational bands, which correspond to: i) shell model configurations, ii) cluster bands with parity inversion doublets and, iii) molecular bands and their parity inversion doublets. The complete list of all observed states in this measurement is given in table 9 for general use.

### 6.1 Shell model states

For the shell model states we can make a list of possible couplings and obtain predictions for the number of states. The following configurations can be considered:

i) The  $^{16}\text{O} \otimes [\nu(sd)^2]$  structure: it is characterized by (2-particle, 0-hole) states with even parity. There are ( $n = 14$ ) possible states with spins 0, 1, 2, 3, 4 and positive parity. A mixing with the cluster states of lower spin can be expected, but this should be small.

Excitations with an even number of proton holes in the  $p$ -shell have been discussed before in connection with the  $\alpha$ -cluster structure. These structures show preferentially the characteristics of collective excitations (with a large number of components of similar strength in the wave function) and are therefore not considered as shell model states.

ii) One-neutron-hole configurations in the  $1p_{1/2}$ -shell: these are negative-parity states. In order to count the possible number of shell model states, we tentatively consider in the spirit of complete spectroscopy the number of shell model states up to (and beyond) the neutron threshold at 8.04 MeV.

The configurations are:

$$\begin{aligned} &(\nu[(1p_{1/2})^{-1}(1d_{5/2})^1] \otimes \nu(2s_{1/2})^2), \\ &(\nu[(1p_{1/2})^{-1}(1d_{3/2})^1] \otimes \nu(2s_{1/2})^2), \\ &(\nu[(1p_{1/2})^{-1}(2s_{1/2})^1] \otimes \nu(1d_{5/2})^2), \\ &(\nu[(1p_{1/2})^{-1}(2s_{1/2})^1] \otimes \nu(1d_{3/2})^2), \end{aligned}$$

and, in addition, mixed configurations for the pair of neutrons in the  $(sd)$ -shell coupled to the  $\nu(1p\text{-}1h)$  excitation, in total more than 34 states. From these configurations with spins from  $0^-$  up to  $7^-$  the list may contain several states also above the neutron threshold, in the continuum.

iii) One-neutron-hole configurations in the  $1p_{3/2}$ -shell: these belong to the higher-lying states with smaller width. Similar to the case ii), we can have more than  $n = 34$  states. The  $(\nu[(1p_{3/2})^{-1}(sd)^1] \otimes \nu(sd)^2)$  configurations were important in the previously discussed OXBASH calculations for the higher-lying members of the  $K^\pi = 1^-$  band shown in fig. 11.

Single-proton excitations  $(\pi[(1p_{1/2})^{-1}(sd)^1] \otimes \nu(sd)^2)$  will contribute in  $^{18}\text{O}$  especially at higher excitation energies. Because of the high binding energy of protons (the proton threshold is at 17.54 MeV) we can expect some narrow states of negative parity at high excitation energies.

### 6.2 Rotational bands, cluster states

The results for rotational bands are summarized in fig. 17. Excitation energies up to 18 MeV are reached for the states of the cluster bands and up to 20.3 MeV for the molecular band. The positive-parity states have mixed configurations or correspond partially to some shell model states with (4p-2h) excitations. The high-lying negative-parity states correspond to the parity inversion partners of the positive-parity cluster bands, they are pure cluster states and are in general well reproduced in cluster model calculations. The negative parity introduces an additional node in the relative motion. Therefore, similar to the negative-parity band in  $^{20}\text{Ne}$ , the  $\alpha$ -particles are well separated from the larger cluster. They will mix with shell model states with particles in higher shells (5p-3h). However, these are very difficult to obtain at the correct excitation energies in the shell model calculations.

Similarly, in the AMD+GCM calculations of Furutachi *et al.* [23], the negative-parity states show a pronounced clustering with a large separation between the clusters. In these calculations the absolute values of the excitation energies are not reproduced (the calculated  $K = 0_2^+$  band starts 2–4 MeV above the  $\alpha$ -threshold depending on the chosen interaction), however, our experimental moments of inertia agree with the predicted values also for the  $K = 0_4^+$  band. These facts confirm the cluster and molecular structure of the bands. The larger deformation of some states at lower excitation energy has been established by the enhanced  $E1$ - $\gamma$ -transitions observed in the work of ref. [17].

There is quite a number of states at higher excitation energies (above 12 MeV), which have not yet been assigned. In this region we should also expect *oblate* shapes, where four  $\alpha$ -particles are placed in a plane with two covalent neutrons shared by all four  $\alpha$ -particles. The threshold in  $^{16}\text{O}$  for the decomposition into four  $\alpha$ -particles is at 14.44 MeV, allowing some binding induced by the valence (two) neutrons, we expect such states in the excitation energy region above 13 MeV. The analogue configuration in  $^{14}\text{C}$  has been identified as a triangular shape of three  $\alpha$ -particles with two neutrons, both experimentally and in calculations [42,43], these states form a  $K^\pi = 3^-$  band with a large moment of inertia. Further states in this excitation energy region must correspond to the  $\sigma$  configurations (or mixed  $\sigma$ - $\pi$ ) of the valence neutrons in the  $K = 0_4^+$  band.

## 7 Conclusions

With the present multi-nucleon transfer reaction it was possible to observe many new states at higher excitation

**Table 9.** Spins and parities  $J^\pi$ , excitation energies  $E_x$ , widths of resonances  $\Gamma$  and cross-sections  $d\sigma/d\Omega$  in the centre-of-mass system at  $10^\circ$ ,  $20^\circ$  and  $39^\circ$  for the present measurement. In the last column are given spins and parities  $J^\pi$ , excitation energies  $E_x$  and widths of resonances  $\Gamma$  from the literature [6].

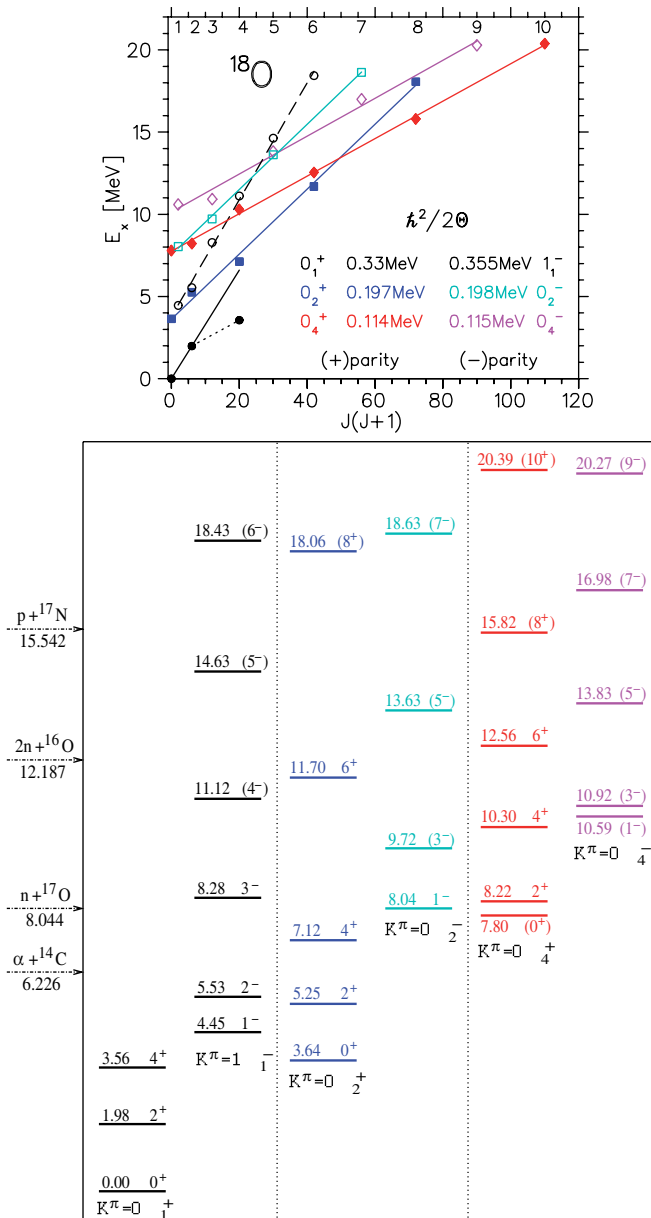
$J^\pi$	$E_x$ [MeV]	$\Gamma$ [keV]	$\left(\frac{d\sigma}{d\Omega}\right)_{cm}$ [ $\mu\text{b}/\text{sr}$ ] $\theta_{lab} = 10^\circ$	$\left(\frac{d\sigma}{d\Omega}\right)_{cm}$ [ $\mu\text{b}/\text{sr}$ ] $\theta_{lab} = 20^\circ$	$\left(\frac{d\sigma}{d\Omega}\right)_{cm}$ [ $\mu\text{b}/\text{sr}$ ] $\theta_{lab} = 39^\circ$	$J_{Lit}^\pi$	$E_{Lit}$ [MeV]	$\Gamma_{Lit}$ [keV]	
$0^+$	0.004(4)		2.82(17)	2.22(20)	0.96(10)	$0^+$	0.000		
	1.980(4)		6.31(25)	7.80(38)	3.00(17)	$2^+$	1.982		
	3.558(4)		2.35(11)	2.80(15)	1.44(10)	$4^+$	3.555		
	3.637(5)		0.28(4)	0.22(4)	0.09(2)	$0^+$	3.634		
	3.919(5)		2.42(12)	2.44(14)	0.92(7)	$2^+$	3.920		
	4.453(5)		1.96(10)	2.32(14)	1.05(8)	$1^-$	4.456		
	5.098(5)		4.93(16)	5.71(22)	2.55(12)	$3^-$	5.098		
	5.254(5)		3.21(13)	3.70(18)	1.91(10)	$2^+$	5.255		
	5.336(5)		1.01(7)	0.92(9)	0.44(5)	$0^+$	5.336		
	5.380(5)		0.62(6)	1.07(9)	0.39(5)	$3^+$	5.378		
	5.531(5)		3.95(15)	3.02(16)	1.37(9)	$2^-$	5.530		
	6.195(5)		1.47(10)	1.02(14)	0.69(8)	$1^-$	6.198		
	6.351(5)		1.46(11)	2.38(13)	1.13(9)	$(2^-)$	6.351		
	6.401(5)		4.27(18)	4.58(17)	0.92(8)	$3^-$	6.404		
						$0^-$	6.880		
		7.115(5)		12.06(30)	12.59(29)	7.39(23)	$4^+$	7.117	
		7.619(5)		0.76(8)	1.25(9)	0.45(6)	$1^-$	7.616	
		7.770(5)		0.76(8)	2.13(12)	1.49(10)	$2^-$	7.771	
		7.796(5)		2.37(13)	2.30(12)	1.26(9)			
		7.857(5)		8.02(25)	14.29(31)	8.15(24)	$5^-$	7.864	
		7.971(5)		9.68(27)	7.30(22)	4.54(18)	$5^-$	7.977	
		8.035(5)		0.43(6)	0.93(8)	0.63(7)	$1^-$	8.038	
		8.129(5)		3.01(15)	4.29(17)	1.85(11)	$5^-$	8.125	
		8.216(5)		20.25(39)	20.51(37)	9.16(26)	$2^+$	8.213	
		8.284(5)		4.34(18)	4.48(17)	2.27(13)	$3^-$	8.282	
		8.414(5)	10	0.43(6)	0.48(6)	0.23(3)	$1^-$	8.410	8
		8.508(5)	5	2.04(12)	2.50(13)	8.86(5)			
							$(4^-)$	8.521	< 50
	8.664(5)	8	1.50(12)	0.66(7)	0.11(2)		8.660		
						$1^+$	8.817	70	
	8.846(5)	33	0.82(9)	1.03(9)	0.33(3)				
							9.03		
	9.053(6)	100	6.12(24)	7.89(24)	4.20(11)				
						$(0, 1, 2)^-$	9.27		
	9.362(5)	37	1.64(12)	2.02(12)	2.11(8)	$2^+$	9.361	27	
							9.414	120	
	9.474(5)	20	0.50(7)	1.01(8)	0.62(4)		9.48	65	
						$(3^-)$	9.672	60	
$(3^-)$	9.715(5)	15	3.26(17)	4.69(18)	2.20(8)	$(5^-)$	9.713	< 50	
							9.890	150	
	10.111(5)	12	1.66(12)	3.28(15)	1.13(6)	$3^-$	10.118	16	
						$(0, 1, 2)^-$	10.24		
	10.293(6)	28	12.97(35)	15.80(33)	9.10(16)	$4^+$	10.295	< 50	
	10.400(7)	30	2.44(15)	2.46(13)	1.56(8)	$3^-$	10.396		
						$(2^-)$	10.43	< 50	

Table 9. Continued.

$J^\pi$	$E_x$ [MeV]	$\Gamma$ [keV]	$\left(\frac{d\sigma}{d\Omega}\right)_{cm}$ [ $\mu\text{b/sr}$ ] $\theta_{lab} = 10^\circ$	$\left(\frac{d\sigma}{d\Omega}\right)_{cm}$ [ $\mu\text{b/sr}$ ] $\theta_{lab} = 20^\circ$	$\left(\frac{d\sigma}{d\Omega}\right)_{cm}$ [ $\mu\text{b/sr}$ ] $\theta_{lab} = 39^\circ$	$J_{Lit}^\pi$	$E_{Lit}$ [MeV]	$\Gamma_{Lit}$ [keV]
(1 <sup>-</sup> )	10.59(1)	70	7.86(27)	12.49(30)	3.92(12)		10.595	
	10.762(8)	10	1.25(11)	1.09(9)	0.83(6)	(2 <sup>-</sup> )	10.67	< 50
							10.82	
(3 <sup>-</sup> )	10.92(1)	30	17.26(40)	17.97(38)	10.69(20)		10.91	
	10.996(6)	29	5.66(23)	3.44(17)	1.89(9)	(2 <sup>-</sup> )	10.99	< 50
						(6 <sup>-</sup> )	11.06	
(4 <sup>-</sup> )	11.115(8)	5	3.84(15)	6.85(24)	3.59(12)		11.13	
	11.423(5)	35		9.66(27)	6.50(15)	(2 <sup>+</sup> )	11.39	
						(4 <sup>+</sup> )	11.41	
						(0, 1, 2) <sup>-</sup>	10.49	
	11.616(8)	25	3.54(14)	10.65(29)	5.04(14)	(2 <sup>-</sup> )	11.52	< 50
	11.702(6)	27	((7.2))	17.38(37)	12.23(20)	5 <sup>-</sup>	11.62	
	11.855(9)	19	3.96(14)	10.24(29)	7.90(18)	6 <sup>+</sup>	11.69	
						(3 <sup>-</sup> )	11.82	
	12.058(6)	12	6.36(18)	6.92(24)	6.27(16)	(2 <sup>-</sup> )	11.90	< 50
	12.118(9)	20	1.70(9)	4.48(19)	2.78(10)	(2 <sup>+</sup> )	12.04	
	12.243(8)	13	5.65(17)	6.75(23)	4.25(13)	(1 <sup>-</sup> , 2 <sup>+</sup> )	12.09	< 50
	12.327(9)	45	3.29(13)	8.12(26)	6.02(14)	(1 <sup>-</sup> )	12.25	
						5 <sup>-</sup>	12.33	
	12.454(7)	24	3.43(13)	6.67(23)	3.44(12)	(3 <sup>-</sup> )	12.41	143
						4 <sup>+</sup>	12.50	
							12.52	< 50
	12.557(7)	24	7.62(20)	12.85(32)	8.28(18)	6 <sup>+</sup>	12.53	
	12.652(8)	25	2.34(11)	5.19(20)	3.22(12)	(2 <sup>-</sup> )	12.66	< 50
	12.711(8)	10	1.50(9)	3.28(16)	2.51(11)			
	12.777(8)	20	1.20(8)	3.17(15)	1.95(9)			
	12.903(7)	73	9.11(20)	9.51(26)	4.08(14)			
	13.001(7)	45	7.43(19)	7.76(24)	6.88(18)	(4 <sup>-</sup> )	12.99	68
	13.098(7)	40	6.09(18)	7.46(23)	5.05(15)	1 <sup>-</sup>	13.1	
	13.262(8)	90	4.80(15)	7.59(24)	4.99(15)			
	13.391(5)	28	2.72(13)	5.49(21)	4.79(14)	(2 <sup>-</sup> )	13.40	108
	13.493(5)	10	3.51(13)	4.37(18)	3.25(10)			
(5 <sup>-</sup> )	13.624(6)	22	16.31(28)	12.97(31)	6.41(17)			
	13.742(7)	3	5.76(17)	4.96(19)				
(5 <sup>-</sup> )	13.82(2)	28	48.77(48)	56.14(64)	36.75(41)	1 <sup>-</sup>	13.8	600
						(6 <sup>-</sup> )	13.85	200
	13.937(6)	17	6.82(18)	7.77(24)	5.24(15)			
	14.161(7)	127	10.22(22)	11.80(29)	11.65(23)	(6 <sup>-</sup> )	14.17	140
	14.433(16)	283	25.05(35)	23.26(41)	14.81(19)		14.45	1070
(5 <sup>-</sup> )	14.63(1)	27	16.94(28)	19.95(38)	9.53(15)			
						1 <sup>-</sup>	14.7	800
	14.803(7)	53	10.04(23)	10.87(28)	3.89(10)			
	14.985(9)	88	10.16(23)	11.32(28)	4.41(10)			
	15.285(9)	28	13.68(27)	18.27(36)	13.34(18)		15.23	300
	15.471(9)	127	8.58(21)	4.57(18)	6.54(13)			
	15.662(8)	40	9.94(23)	11.69(29)	9.38(15)			

Table 9. Continued.

$J^\pi$	$E_x$ [MeV]	$\Gamma$ [keV]	$\left(\frac{d\sigma}{d\Omega}\right)_{cm}$ [ $\mu\text{b}/\text{sr}$ ] $\theta_{lab} = 10^\circ$	$\left(\frac{d\sigma}{d\Omega}\right)_{cm}$ [ $\mu\text{b}/\text{sr}$ ] $\theta_{lab} = 20^\circ$	$\left(\frac{d\sigma}{d\Omega}\right)_{cm}$ [ $\mu\text{b}/\text{sr}$ ] $\theta_{lab} = 39^\circ$	$J_{Lit}^\pi$	$E_{Lit}$ [MeV]	$\Gamma_{Lit}$ [keV]
$(8^+)$	15.810(10)	20	31.40(40)	46.64(57)	29.26(27)	$1^-$	15.8	700
	15.981(9)	87	20.10(32)	18.81(36)	11.74(17)		15.95	< 50
	16.111(8)	150	8.40(21)	9.77(26)	5.71(14)			
	16.333(7)	33	8.25(21)	6.80(19)	8.17(16)	$1(-)$	16.210	
	16.425(9)	113	31.40(23)	46.64(12)	29.26(12)	$(3, 2)^-$	16.315	
	16.721(12)	217	25.41(35)	19.49(32)	16.67(22)	$2^-$	16.399	< 20
						$(2^-, 4^-)$	16.210	< 50
$(7^-)$	16.99(1)	50	20.70(32)	23.13(34)	12.24(20)	$(3, 2)^-$	16.948	
	17.163(15)	283	36.50(42)	38.89(44)	22.40(27)	$(3^-)$	17.025	20
	17.430(8)	69	13.06(25)	10.84(23)	4.92(13)	$(7^-)$	17.05	350
						$1^-$	17.398	600
						$(2, 1, 3)^-$	17.45	
						$(4^-)$	17.46	600
						$(4^-)$	17.5	150
	17.568(12)	150	12.73(25)	11.20(24)	5.93(14)	$(1, 2, 3)^-$	17.502	
	17.718(15)	142	17.01(29)	17.77(30)	9.71(18)	$(8^+)$	17.6	
							18.049	4300
$(8^+)$	18.058(8)	83	19.35(30)	21.49(35)	12.45(20)		18.2	
	18.198(7)	25	6.88(20)	4.94(16)	3.27(10)			
$(6^-)$	18.43(1)	16	15.16(30)	10.07(23)	5.75(14)	$(3^-)$	18.45	
							18.5	
$(7^-)$	18.630(10)	100	29.92(42)	35.75(44)	23.36(26)			
	18.721(10)	140	50.88(55)	46.76(50)	24.17(28)			
						$1^+$	18.871	
						$(1, 2^+)$	18.927	
	19.028(10)	247	54.43(57)	54.65(54)	28.17(30)	$(7^-)$	18.95	350
						$(1, 3)^-$	19.027	
							19.24	< 20
	19.431(11)	213	26.04(39)		5.47(16)	$1^-$	19.4	900
	19.597(13)	70	11.36(26)		19.57(31)			
	19.695(10)	85	18.30(37)		12.87(25)		19.7	200
	19.918(17)	80	9.15(26)		7.11(19)		20.2	180
$(9^-)$	20.28(3)	120	21.08(39)		16.12(28)			
$(10^+)$	20.385(12)	165	45.07(57)		19.34(31)	$(7^-)$	20.36	< 20
	20.753(10)	110	17.33(35)					
							20.86	97
							21.0	150
	21.181(16)	190	43.72(56)					



**Fig. 17.** (Color online) Overview for all the band structures observed in  $^{18}\text{O}$ . Upper part: plot of all bands discussed in this work in a diagram of excitation energies  $E_x$  vs.  $J(J+1)$ . Lower part: level diagrams for the discussed six bands of  $^{18}\text{O}$ . Left column:  $K^\pi = 0_1^+$  ground-state band and the  $K^\pi = 1_1^-$  band; central column: members of the  $K^\pi = 0_2^\pi$  inversion doublet bands; column on the right: members of the  $K^\pi = 0_4^\pi$  inversion doublet bands.

energy in  $^{18}\text{O}$ . Although spin assignments were not possible directly, we were able to use cross-sections and excitation energy systematics to establish six bands, where four rotational bands form two parity doublets with internal cluster structure. Figure 17 gives an overview of all bands in  $^{18}\text{O}$ : the upper part shows a plot of excitation energies in dependence on  $J(J+1)$  together with the moments of inertia  $\Theta$  (in the figure the values of  $\hbar^2/2\Theta$  are given). These values correspond to distinctly large deformations

according to the cluster structure suggested in fig. 1. In the lower part of fig. 17 the level diagrams for the six bands of  $^{18}\text{O}$  are plotted separately.

We may also conclude that the strongly bound  $^{14}\text{C}$  nucleus has equivalent properties as an  $^{16}\text{O}$  cluster, as mentioned already in the introduction. Therefore the Ikeda diagram [1] and extended Ikeda diagram with valence neutrons [5] must be revised to include also the  $^{14}\text{C}$  cluster. For the latter, the study of bands in  $^{20}\text{O}$  by Furutachi *et al.* [23] clearly establishes parity inversion doublets predicted for the  $^{14}\text{C} \otimes ^6\text{He}$  cluster and  $^{14}\text{C} \otimes 2n \otimes \alpha$  molecular structures.

The technical staff at MLL is gratefully acknowledged for the stable operation of the accelerator with the high-current  $^7\text{Li}$  beam.

## References

1. H. Horiuchi, K. Ikeda, Prog. Theor. Phys. (Jpn.) **40**, 277 (1968).
2. W. von Oertzen, M. Freer, Y. Kanada-En'yo, Phys. Rep. **432**, 43 (2006).
3. W. von Oertzen, Z. Phys. A **354**, 37 (1996).
4. W. von Oertzen, Z. Phys. A **357**, 355 (1997).
5. W. von Oertzen, Eur. Phys. J. A **11**, 403 (2001).
6. D.R. Tilley, H.R. Weller, C.M. Cheves, R.M. Chasteler, Nucl. Phys. A **595**, 1 (1995) and updates (2000).
7. G.L. Morgan *et al.*, Phys. Lett. B **32**, 353 (1970).
8. H.T. Fortune, L.R. Medsker, J.N. Bishop, Nucl. Phys. A **309**, 221 (1978).
9. A. Cunsolo *et al.*, Phys. Rev. C **24**, 476 (1981).
10. A. Cunsolo *et al.*, Phys. Lett. B **112**, 121 (1982).
11. M. Gai *et al.*, Phys. Rev. Lett. **50**, 239 (1983).
12. K.P. Artemov *et al.*, Sov. J. Nucl. Phys. **37**, 805 (1983).
13. K.P. Artemov *et al.*, Yad. Fiz. **37**, 1351 (1983).
14. G.L. Morgan *et al.*, Nucl. Phys. A **148**, 480 (1970).
15. N. Curtis *et al.*, Phys. Rev. C **66**, 024315 (2002).
16. H.T. Fortune, Phys. Rev. C **18**, 1053 (1978).
17. M. Gai *et al.*, Phys. Rev. C **43**, 2127 (1991).
18. V.Z. Goldberg *et al.*, Phys. At. Nucl. **68**, 1079 (2005).
19. R.L. Lawson *et al.*, Phys. Rev. C **14**, 1245 (1976).
20. G. Lévai, J. Cseh, W. Scheid, Phys. Rev. C **46**, 548 (1992).
21. G. Reidemeister, F. Michel, Phys. Rev. C **47**, R1846 (1993).
22. P. Descouvemont, D. Baye, Phys. Rev. C **31**, 2274 (1985).
23. N. Furutachi *et al.*, Prog. Theor. Phys. **119**, 403 (2008).
24. N. Itagaki, M. Kimura, Phys. Rev. C **79**, 034312 (2009).
25. T. Dorsch, PhD Thesis, Technical University München (2008).
26. M. Löffler, H.J. Scheerer, H. Vonach, Nucl. Instrum. Methods **111**, 1 (1973).
27. H.F. Wirth, PhD Thesis, Technical University München (2001).
28. H.G. Bohlen, *Spectra Analysis Code SPEC (version F)*, HMI Berlin, private communication (2003).
29. R. Sherr, H.T. Fortune, Phys. Rev. C **58**, 3292 (1998).
30. G. Herzberg, *Molecular Spectra and Molecular Structure*, Vol. **I**, *Spectra of Diatomic Molecules* (van Nostrand, Princeton, 1950).

31. A. Bohr, B.R. Mottelson, *Nuclear Structure*, Vol. **II** (World Scientific, 1998).
32. W. Nazarewicz *et al.*, Phys. Rev. Lett. **52**, 1272 (1984).
33. W. Nazarewicz, P. Olanders, Nucl. Phys. A **441**, 420 (1985).
34. P.A. Butler, W. Nazarewicz, Rev. Mod. Phys. **68**, 350 (1996).
35. W. Bauhoff *et al.*, Phys. Rev. C **29**, 1046 (1984).
36. M. Kimura, Phys. Rev. C **69**, 044319 (2004).
37. B. Buck, C.B. Dover, J.P. Pilt, Nucl. Phys. A **290**, 205 (1977).
38. W. Rae, A. Etchegoyen, B.A. Brown, *OXBASH, The Oxford-Buenos Aires-MSU shell-model code*, Technical Report 524 (Michigan State University Cycl. Lab., 1985).
39. E.K. Warburton, B.A. Brown, Phys. Rev. C **46**, 923 (1992).
40. N.I. Ashwood *et al.*, J. Phys. G **32**, 463 (2006).
41. I. Thompson, *Coupled reaction channel code FRESKO*, private communication.
42. W. von Oertzen *et al.*, Eur. Phys. J. A **21**, 193 (2004).
43. N. Itagaki *et al.*, Phys. Rev. Lett. **92**, 142501 (2004).